International Journal of Electrical, Electronic and Communication Sciences
ISSN: 2517-9438
Vol:4, No:8, 2010

A Multi-Radio Multi-Channel Unification Power Control for Wireless Mesh Networks

T. O. Olwal, K. Djouani, B. J. van Wyk, Y. Hamam, and P. Siarry

***Abstract*—**Multi-Radio Multi-Channel Wireless Mesh Networks (MRMC-WMNs) operate at the backbone to access and route high volumes of traffic simultaneously. Such roles demand high network capacity, and long "online" time at the expense of accelerated transmission energy depletion and poor connectivity. This is the problem of transmission power control. Numerous power control methods for wireless networks are in literature. However, contributions towards MRMC configurations still face many challenges worth considering. In this paper, an energy-efficient power selection protocol called PMMUP is suggested at the Link-Layer. This protocol first divides the MRMC-WMN into a set of unified channel graphs (UCGs). A UCG consists of multiple radios interconnected to each other via a common wireless channel. In each UCG, a stochastic linear quadratic cost function is formulated. Each user minimizes this cost function consisting of trade-off between the size of unification states and the control action. Unification state variables come from independent UCGs and higher layers of the protocol stack. The PMMUP coordinates power optimizations at the network interface cards (NICs) of wireless mesh routers. The proposed PMMUP based algorithm converges fast analytically with a linear rate. Performance evaluations through simulations confirm the efficacy of the proposed dynamic power control.

***Keywords*—**Effective band inference based power control algorithm (EBIA), Power Selection MRMC Unification Protocol (PMMUP), MRMC State unification Variable Prediction (MRSUP), Wireless Mesh Networks (WMNs).

I. Introduction

WIRELESS Mesh Networks (WMNs) have emerged as a ubiquitous part of modern broadband communication networks [1]. In WMNs, nodes are composed of wireless mesh clients, routers (e.g., mesh points) and gateways. Wireless mesh routers or mesh points (MPs) form a multi-hop wireless network which serves as a backbone to provide network access to mesh clients. As a result wireless backbone nodes convey a large amount of traffic generated by wireless clients to a few nodes that act as gateways to the Internet. In order to meet high traffic demands, wireless backbone nodes (e.g., MPs) can be equipped with multiple radios and/or operate on multiple orthogonal frequency channels (or band) [24]. In addition, WMN routers form a self-managing and dynamic system. It can adapt to nodes entering the network or those exiting it due to node failure, poor connectivity and so forth. This implies that WMNs have low up-front cost, are easy to maintain, are robust and have reliable service coverage [28]. WMN deployments have recently been picked up in cities, urban and rural communities. WMN offers excellent framework for delivering broadband internet services, and distributed information sharing and storage to such areas.

Many works [2], [5], [29] have emphasized the traffic carrying capacity of the wireless backbone as the main design concern. Power control has been treated as a secondary issue at the backbone nodes [25]. The reason is that mesh routers in many applications are usually stationary and directly connected to an electric outlet. However, the transmission power control in wireless multi-radio multi-channel (MRMC) systems resolves: connectivity and inter (intra) channel interference problems, and the battery power limitations in remote applications [28]. Selecting an appropriate transmission power level allows mesh traffic to navigate path obstacles using short multiple hops over wireless medium [30].

In order to make such MRMC configurations work as a single wireless router, a *virtual* medium access control (MAC) protocol is needed on top of the legacy MAC [1]. The virtual MAC should coordinate (unify) the communication in all the radios over multiple non-overlapping channels [25]. This unification protocol should hide the complexity of multiple network interface cards (NICs) at the MAC and physical layers from the upper layers. The first Multi-radio unification protocol (MUP) was reported in [25]. MUP discovers neighbours, selects the NIC with the best channel quality based on the round trip time (RTT) and sends data on a pre-assigned channel. MUP then switches channels after sending the data. However, MUP assumes power unconstrained mesh network scenarios. That is, mesh nodes are plugged into an electric outlet. MUP utilizes only a single selected channel for data transmission.

Instead of MUP, this paper considers an energy-efficient power selection multi-radio multi-channel unification protocol (PMMUP) [34]. PMMUP enhances functionalities of the original MUP. Such enhancements include: an energy-aware efficient power selection capability and the utilization of parallel radios over power controlled non overlapping channels to send data traffic simultaneously. That is, PMMUP resolves the need for a single MP node (wireless mesh router) to access mesh client network and route the backbone traffic

T. O. Olwal is with the Tshwane University of Technology, Paris-Est University and Meraka Institute at the CSIR, South Africa. Phone: +27 12 841 2085; +27128414829; thomas.olwal@gmail.com.

B. J. van Wyk, K. Djouani and Y. Hamam, are with Tshwane University of Technology, French South African Institute of Technology, X680, Pretoria (e-mail: vanwykb@gmail.com,djouani@univ-paris12.fr, hamamy@esiee.fr).

P. Siarry is with the University of Paris-Est. (siarry@univ-paris12.fr).

simultaneously [1]. Like MUP, the PMMUP requires no additional hardware modification. Thus, the PMMUP complexity is comparative to that of the MUP. PMMUP mainly coordinates local power optimizations at the NICs, while NICs measure local channel conditions. To achieve this, every PMMUP layer exploits the upper network layer information to divide the entire multiple channels WMN into a set of disjoint unified channel graphs (UCGs) [21]. A UCG is a set of radio interfaces (NICs) that are interconnected to each other via a common wireless medium channel. NICs belonging to the same UCG optimize their transmission powers and communicate to each other when there are pending packets at their queues. PMMUP sets initial unification variables such as energy reserves and coordinated states from other UCGs, NICs *predict* states from a lower level local channel network (UCG), PMMUP *updates* unification variables and NICs *compute* optimal transmission power levels based on the predicted states. This guess, predict, update and compute (GPUC) model may be synchronously or asynchronously executed. Synchronous executions require all NICs to terminate optimal power executions within a common coordinated time. On the other hand, asynchronous executions allow each NIC or user to iterate at autonomous pace [13]. Because these power control algorithms are coordinated by the PMMUP, we refer to them as PMMUP based algorithms.

The rest of this paper is organized as follows: Section II presents related work. The MRMC-WMN model is characterized in Section III. In Section IV, we design and analyse a Large-Scale Multi-Radio System Controller. Section V presents the Simulation Set-up and Results. Finally, Section VI concludes the paper.

II. Related Work

In this paper, the power control technique exploits classical linear quadratic control models [20], [13], [12]. This is because optimal quadratic control represents the trade-off between the size of the states and the control action i.e., power level decision. Such modelling techniques have been liberally applied to parallel and distributed wire-line computer networks [15]. However, interference-limited communication or code division multiple access (CDMA) schemes in wireless networks still pose major challenges [14], [30]. We believe that state-space modelling and consequently linear quadratic power control schemes can address transmission power control issues in complex dimensions of MRMC configurations. Related to our model approach is the work by Subramanian and Sayed [8]. The authors proposed the distributed joint rate and power control for single channel wireless networks. They modelled network dynamics in terms of linear state-space models by changing variables from linear scale to logarithmic scale. They then invoked quadratic control strategies to jointly control the power and data rate in the network. However, they focused on signal-to-interference plus noise ratio (SINR) performance criteria at a *common base station* receiver. Common base stations are not feasible for fully distributed backbone WMNs. That is, WMN self-management requires autonomous stations [9]. Furthermore, the authors studied a special case of single radio interface system. Neely *et al.* [6] studied dynamic power control allocation and routing for time-varying wireless networks. However, the design follows linear programming (LP) optimization techniques in which the network scope global information is available at each node. The knowledge of global information incurs message overhead costs and thus not feasible in a self-managing WMN [1]. Ata [23] proposed an objective function that minimizes the long-run average energy consumption subject to quality of service (QoS) constraint. In order to solve this minimization problem, a controller that dynamically chooses a queue state-dependent transmission rate by varying transmission power over time was developed [23]. In [14], Koskei and Gajic proposed optimal signal to interference ratio (SIR)-based power control strategies for a distributed uplink cellular communication systems. The authors defined a cost function for each mobile node that consists of a weighted sum of power, power update, and SIR deviation. However, their work addressed a single radio single channel system. Autonomous interference estimation based closed loop power control for single radio wireless networks have been reported in [10], [11]. In this case, users dynamically allocate transmit power so as to minimize an objective function consisting of the user's performance degradation (i.e., expressed in terms of the received SIR deviation) and the network interference (i.e., expressed as a gross network interference). However, methods are single radio based and the scalability with multiple radios can not be guaranteed [9]. Cross-layer transmission power optimizations for single channel wireless networks can be found in [3],[30]. Joint transmission power and cross-layer resource allocations are severely complex problems when considering multiple radios multiple channels (MRMC). Several transmission power controlled protocol schemes have been studied with the aim to minimize medium access interference [31]-[33]. In [31], a scheme that provides a good trade-off between throughput, energy and fairness is provided. In [32], an adaptive transmission power controlled medium access control (ATPMAC) scheme is suggested, while the use of power controlled dual channel to avoid interference has been investigated in [33]. Their main drawback is that such works do not consider effects of cross-channel interference in fading wireless channels. Fading wireless channels violate orthogonality of multiple frequency channels [7], [12].

This is why we propose a multi-level power control based on the PMMUP at the link layer [34]. Based on the multiple link states [34], we incorporate unification variables. We have also provided rigorous convergence analysis of the proposed algorithm. The key simulation results are faster algorithm convergence, low power consumption and significant throughput improvement for the backbone WMNs.

III. System Model

A. Preliminaries and Assumptions

Consider a wireless MRMC multi-path and multi-hop WMN (See Fig. 1 and Fig. 2), operating under dynamic network conditions [6]. Let us assume that the entire multiple channels mesh network is virtually divided into L UCGs each of which contains all nodes in the network. In each UCG there

are $\|V\| = N_V$, NICs (communication radio interfaces (RIs)) that connect to each other possibly via multiple hops [21].

This means that each multi-radio mesh point (MP) node is a member of at least one UCG. For simplicity, we can assume that the number of NICs in each MP node is at most the number of UCGs associated to that node, i.e., $\|T_A\| \le \|L_A\|$. Each UCG forms a subsystem with wireless links (users) as its members. Power resources are dynamically allocated by every user depending on intra and inter-subsystem (UCG) state coordination via the PMMUP layer. PMMUP resolves the greedy competition for common memory, central processor and energy supply modules among multiple users associated by a particular node [10].

Let us assume that there exists an established logical topology, where some devices belonging to a certain UCG are *sources* of transmission say $i \in T_A$ and some devices act as 'voluntary' *relays*, say $r \in T_B$ to *destinations*, say $d \in T_C$. A sequence of connected *logical links* or simply channels $l \in L(i)$ forms a *route* originating from source i. It should be noted that each asymmetrical physical link may need to be regarded as multiple logical links due to multiple channels [3]. The system model assumes that each NIC accesses tuneable channels denoted as $l \in L(i)\ \forall l$ after transmission time slot duration. Time slot durations are assumed fixed [11]. Each time slot accounts for a power control adjustment mini-slot time, a packet transmission mini-slot time and a guard time interval. For analytical convenience time slots will be normalized to integer units $t \in \{0,1,2,\ldots\}$ with only a fraction of time slot dedicated for power optimization. Moreover, channels will be assumed to be statically assigned by the Link-Layer. The reason is that dynamic channel assignments within every time slot incur run time overhead costs [29].

Table I and Table II summarize the definitions of the notations and abbreviations, respectively used throughout in this sequel.

TABLE I
TABLE OF NOTATIONS

$I_{-i,l}^{ACI}(t)$	Net adjacent lth channel interference for ith user at time t
$p_{i,l}(t+1)$	Predicted transmission power for ith user on lth UCG in slot $t+1$
$e_\beta(t+1)$	Signal-to-interference plus noise ratio (SINR) deviation for ith user on lth UCG in slot $t+1$
$e_I(t+1)$	Aggregate Interference deviation during slot $t+1$
$e_\Gamma(t+1)$	The lth link rate deviation for ith user during slot $t+1$
$\mathbf{x}_l(t)$, $\mathbf{x}_l(t+1)$	The lth link state vector and interaction state vector
$\mathbf{X}$ and X	Denotes a matrix notation and a random variable
$\mathbf{u}$	Power control input signal
$\mathbf{P}$	Discrete Riccati Regulator idempotent matrix
$\mathbf{y}$	Linear combination of states from other UCGs to lth UCG
$\boldsymbol{\varphi}$ and $\boldsymbol{\pi}$	State unification vector and state weighting vector available to ith user

TABLE II
TABLE OF ABBREVIATIONS

CV	Coordination Variables from PMMUP layer
EBIA	Effective Band (channel) Interference Estimation based power control algorithm
IV	Interaction Variable between channels
MRMC	Multiple radios multiple channels
MRSUPA	MRMC unification asynchronous state prediction Algorithm
MRSUPS	MRMC unification synchronous state prediction Algorithm
NIC	Network Interface Card or radio device
PMMUP	Power Selection MRMC Unification Protocol
UCG	Unified Channel Graph
UV	Unification Variables from Upper Layers

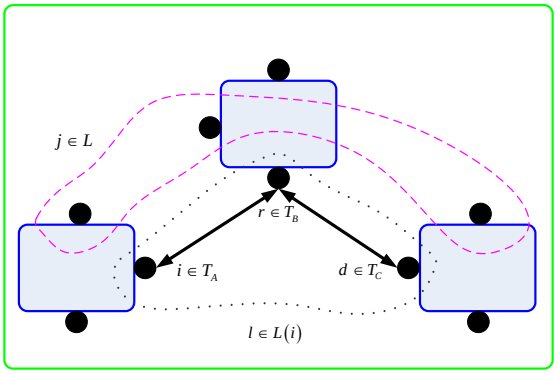

Fig. 1: MRMC multi-hop WBMN:
Each Mesh Router is assumed to have a single power supply. Node A has $\|T_A\|$ network interface cards (NICs) and $\|L_A\|$ non-overlapping frequency channels. Node B and C have, $\|T_B\|$ and $\|T_C\|$ NICs, respectively. Source NIC i can communicate to destination device d through multiple hop relays (routers), i.e., r. Devices can switch between different channels so that each channel is maximally utilized most of the time. However, the criterion of channel switching depends on the channel with the best channel quality as observed by the Link-Layer [25].

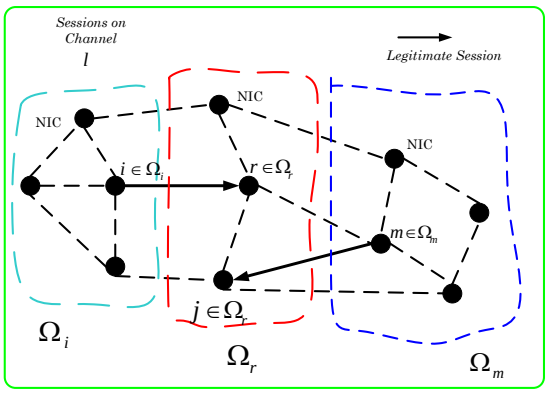

Fig. 2: Interference Model for ith transmission in a multi-hop UCG network

B. Adjacent Channel Interference Estimation and Basic Power Control

If during time slot t NIC $i \in T_A$ on channel $l \in L(i)\ \forall l$ randomly selects a transmission power $p_i^r(t) \in \Pi_i$ to multicast pending packets in its queue $q_i(t) > 0$ to a set of relaying

devices, say $r \in T_B$ on channel $l \in L(i)$ then its transmission interferes with simultaneous transmissions in its neighbourhood (i.e., well known exposed terminal problem [17]). Terminals, say $m \in \Omega_m$ transmitting to terminal $j \in \Omega_r$ (see Fig. 2) at time slot t cause interference at NIC r. The net instantaneous co-channel interference (CCI) at the beginning of time slot t at device r is given as in [6]. The net instantaneous adjacent channel interference (ACI) against the ith terminal transmission is estimated by:

$$I_{-i,l}^{ACI}(t) = \sum_{m \in \Omega_m, m \neq i} G_{m,l}^{r}(t) \sum_{l \in \{1,..L\}} \sum_{\substack{j \in \Omega_r \\ q_{m,l}>0,\, x_{m,l}^{r}>0}} c_{im} p_{m,l}^{j}(t) + c_{im} x_m^j \delta\left(p_{m,l-1}^{j}(t) + p_{m,l+1}^{j}(t)\right)$$
$$- G_{i,l}^{r}(t) \sum_{l \in \{1,...L\}} \sum_{\substack{j \in \Omega_r \\ j \neq r}} x_{i,l}^{j}\, p_{i,l}^{j}(t) + \delta x_i^j \left(p_{i,l-1}^{j}(t) + p_{i,l+1}^{j}(t)\right) + \eta_{r,l}(t)$$
$$= I_{r,l}^{ACI}(t) - G_{i,l}^{r}(t) \sum_{l \in \{1... L\}} P_{i,l}^{sum}(t) + \eta_{r,l}(t), \qquad (1)$$

Here, $G_{m,l}^{r}(t), G_{i,l}^{r}(t) \in \Re$ are asymmetrical wireless channel gains from senders m and i, respectively to receiver r on the UCG l. The coding orthogonality coefficients at the senders are $c_{im}(t) \in \Re$ and the CDMA schemes are assumed [14]. The transmission activity constraints are $x_{m,l}^{j}(t), x_{i,l}^{j}(t) \in \{0,1\}$. These constraints depict an actively transmitting or backing-off network user. The thermal noise at the receiver r is $\eta_{r,l}(t) \in \Re$. The transmission power leakage factor between neighbouring adjacent channels is $0 \leq \delta \leq 1$.

Such ACI and channel gain estimates are gathered by each NIC using a fraction of maximum transmission power called probing power level [6]. Indeed, in IEEE 802.11 wireless standards, channel probing is achieved through request-to-send and clear-to-send (RTS/CTS) message exchanges [17]. Such mechanisms allow NICs to sense whether the channel between the sender and the receiver pair is busy or not. The work in [4] exploited this protocol to extend the closed loop dynamic power control in [10]. Thus, the so called effective band interference (EBI) estimation based dynamic power control algorithm (EBIA) was derived [4],[10]. EBIA is given by

$$p_{i,l}(t+1) = \begin{cases} p_{i,l}(t) + \alpha_{i,l}(t) I_{(i,r),l}(t) & \text{if } q_{i,l}(t) > 0 \\ 0, & \text{otherwize} \end{cases}, \qquad (2)$$

where EBI is denoted as $I_{(i,r),l}(t) \triangleq \varsigma I_{i,l}(t) + (1-\varsigma) I_{r,l}(t)$, for $0 \leq \varsigma \leq 1$. The basic idea is that each transmitter and receiver pair (user) autonomously estimates interferences at both the receiver and sender during each time slot [4], [10]. This is in order that a node can choose power levels judiciously so as not to interrupt legitimate active sessions in its neighbourhood. Moreover, hidden terminal nodes at the receiver can be exposed so that an appropriate transmission power level is selected by the sender. Finally, we define the feedback control gain $\alpha_{i,l}(t) \in \Re$ in equation (2) as a time-variant sequence [10]. This is because the channel quality is assumed to change from one time slot to the other. The well known Kalman filter is adopted to evaluate the feedback control gain [7].

It is worth noting from (2) that if there exists packets in a queue, i.e., $q_{i,l}(t) > 0$ then a device (NIC) decides to transmit with one step predicted power levels, i.e., $p_{i,l}(t+1) \geq 1$. Otherwise it decides to back-off, i.e., $p_{i,l}(t+1) = 0$. Back-off sessions save transmission power significantly. Thus, back-off sessions will form part of energy-efficient strategy in our proposed scheme. Deciding on whether to transmit with what power, impacts jointly on the desired received SINR, interference level and or congestions caused to network users, transmission rate on a given wireless link [6]. This is the synergy of cross-layer based power optimization [3].

This paper extends the dimension of the problem addressed in (2). It investigates the autonomous transmission power selection sequence $\{p_l(t)\}$ so that: the received SINR target is satisfied, the aggregate network interference is minimized [10], the queuing backlogging is minimized [5], and the appropriate network density is maintained [19]. Also, the scheduled transmission data rate should not exceed the wireless link capacity offered [6], [9]. Consequently, we define the autonomous cross-layer based power control law of a logical user on UCG l as

$$p_l(t+1) = \begin{cases} p_l(t) + f_l(\mathbf{x}) & \forall \mathbf{x} \in \{\mathbf{x}\} \quad \text{if } q_l(t) > 0 \\ 0, & \text{otherwise} \end{cases} \qquad (3)$$

where $f_l(\mathbf{x}) = f_l(\beta_l(t), I_l(t), \Gamma_l(t))$, with $\beta_l(t)$, $I_l(t)$ and $\Gamma_l(t)$ as the actual SINR, aggregate network interference and scheduled transmission rate during time slot t. It should be noted that $f_l(\mathbf{x})$ is a nonlinear function of cross layer inter (intra) channel states [29]. Such states are assumed available to each network interface card (NIC) at the beginning of each time slot through channel probing [6]. Using the Taylor series to obtain a first order linear approximation to $f_l(\mathbf{x})$ gives

$$f_l(\mathbf{x}) \triangleq f\left(\gamma_l^{ss}, I_l^{ss}, \Lambda_l^{ss}\right) + \alpha_\beta\left(\beta_l(t) - \gamma_l^{ss}\right) + \alpha_I\left(I_l(t) - I_l^{ss}\right)$$
$$+ \alpha_\Gamma\left(\Gamma_l(t) - \Lambda_l^{ss}\right) \qquad (4)$$

where $\lim_{t\to\infty} \frac{1}{t} \sum_{\tau=0}^{t-1} \beta_l(\tau) = \gamma_l^{ss}$ denotes the steady state value of actual SINR $\beta_l(t)$, $\lim_{t\to\infty} \frac{1}{t} \sum_{\tau=0}^{t-1} I_l(\tau) = I_l^{ss}$ denotes the steady state value of actual network interference $I_l(t)$ and $\lim_{t\to\infty} \frac{1}{t} \sum_{\tau=0}^{t-1} \Gamma_l(\tau) = \Lambda_l^{ss}$ denotes the steady state value of the scheduled transmission data rate $\Gamma_l(t)$ through router device r on UCG l with probability one. The parameters α_β, α_I, and α_Γ are assumed known constants [4]. Queue dynamics in

(3) are modelled as in [3], [5]. The exogenous or endogenous packets arriving at the individual relaying NICs are assumed poison distributed [6]. An admission control mechanism [5] is exploited to accept or drop a new arriving packet depending on the buffer capacity $B_l(t)$ in bits [6].

C. State Space Model

Our main task is to design the power control sequence $\{p_l(t)\}$ such that network state dynamic sequences $\{\mathbf{x}_l(t)\}$ are derived to steady states [14],[12]. Introducing the state space transition model representation, we have:

$$\mathbf{x}_l(t) \triangleq \left(\beta_l(t)-\gamma_l^{ss} \quad I_l(t)-I_l^{ss} \quad \Gamma_l(t)-\Lambda_l^{ss}\right)^T.$$

Based on state equations we showed in [34], one can obtain

$$\mathbf{x}_l(t+1) = \mathbf{A}_l(t)\mathbf{x}_l(t) + \mathbf{B}_l(t)\mathbf{u}_l(t) + \varepsilon_l(t), \quad (5)$$

where $\mathbf{A}_l(t) = \begin{pmatrix} \frac{m}{n}H\alpha_\beta & \frac{m}{n}H\alpha_I & \frac{m}{n}H\alpha_\Gamma \\ mG\alpha_\beta & mG\alpha_I & mG\alpha_\Gamma \\ \frac{\alpha_\beta}{p_l} & \frac{\alpha_I}{p_l} & \frac{\alpha_\Gamma}{p_l} \end{pmatrix}(t)$ and

$\mathbf{B}_l(t)\mathbf{u}_l(t) = \begin{bmatrix} u_\beta(t) \\ u_I(t) \\ u_\Gamma(t) \end{bmatrix}$ characterizes the control sequence that need to be added to $p_l(t+1)$ equation (3) in order to derive network dynamics to steady states. $\mathbf{B}_l(t)$ is assumed to be a 3 x 1 coefficient matrix. The state stochastic shocks term $\varepsilon_l(t)$ is a 3 x 1 random vector with zero mean and covariance matrix

$$\Theta_\varepsilon = \mathrm{E}\varepsilon_l(t)\varepsilon_l^T(t) = diag\left(\sigma_\beta^2, \sigma_I^2, \sigma_\Gamma^2\right). \quad (6)$$

From (5), driving the SINR deviation and link rate deviation to as minimal as possible benefits the individual user [4]. On the other hand, ensuring low aggregate network interference is beneficiary to network users [10]. It is crucial that each user selects the transmission power sequence so as to maintain state transitions as minimal as possible. This can be achieved by weighting the state vector as

$$\boldsymbol{\omega}^T \mathbf{x}_l(t) \triangleq \tilde{\mathbf{x}}_l(t), \quad (7)$$

where $\boldsymbol{\omega}^T = (\omega_{l1} \quad \omega_{l2} \quad \omega_{l2})$ are weights assigned to users by the PMMUP according to the available battery energy [10]. Intuitively, when $\omega_{l1} > \omega_{l2}$ then it implies availability of more energy resource. Users adjust powers increasingly to maintain the desired SINR and queue size level. Conversely, when $\omega_{l2} > \omega_{l1}$ then it implies energy supply shortage. Users judiciously adjust transmission power to keep the network interference as low as possible. For convenience, we define $\omega_l = \omega_{l2} / \omega_{l1} \in \Re^+$ such that $\omega_l \in [0, \infty] \ \forall l$.

IV. MRMC Wireless System Controller

If at each wireless mesh router there are N network interface cards (NICs) tuneable to L orthogonal channels (UCGs) then at each node the state space equation (5) becomes

$$\tilde{\mathbf{x}}(t+1) = \mathbf{A}(t)\tilde{\mathbf{x}}(t) + \mathbf{B}(t)\mathbf{u}(t), \quad \tilde{\mathbf{x}}(0) = \tilde{\mathbf{x}}_0, \quad (8)$$

where $\tilde{\mathbf{x}} \in \Re^{3N}$, $\mathbf{u} \in \Re^M$, $\mathbf{A} \in \Re^{3N \times 3N}$, $\mathbf{B} \in \Re^{3N \times M}$ and M is the size of the control input vector.

We note from (8) that: first, the structural complexity of the MRMC system increases with the sizes of NICs, channels (UCGs), and control input vector. Second, the number of NICs on one router may be different with that of another router i.e., heterogeneity, in the WMN [1], [24]. Third, due to diverse fading conditions, state dimensions may vary from one UCG to the other. Therefore, power optimizations executed between multi-radio nodes may be complex and impractical with large system dimensions. Consequently (8) is decomposed into N interconnected subsystems (network users) each of dimension three as was given by (5). Because only active radio on a pre-assigned channel performs power control, we set $L = N$ as a worst case scenario. The simplified multi-radio multi-channel state space (MMSS) model representation becomes [13], [20].

$$\tilde{\mathbf{x}}_i(t+1) = \mathbf{A}_i(t)\tilde{\mathbf{x}}_i(t) + \mathbf{B}_i(t)\mathbf{u}_i(t) + \mathbf{C}_i(t)\mathbf{y}_i(t) + \varepsilon_i(t)$$
$$\tilde{\mathbf{x}}_i(t_0) = \tilde{\mathbf{x}}_{i0}, \ \forall i \quad (9)$$

where $\mathbf{y}_i(t)$, introduced in (9), is a linear combination of states (LCS) from other UCGs available to the ith network user belonging to UCG l. This LCS is defined as

$$\mathbf{y}_i(t) = \sum_{\substack{j=1 \\ j \neq i}}^{N} \mathbf{L}_{ij}(t)\tilde{\mathbf{x}}_j(t) + \varepsilon_i^y(t), \quad (10)$$

where $\varepsilon_i^y(t)$ denotes the coordination process shocks with zero mean and the covariance matrix is denoted as $\Theta_\varepsilon = \mathrm{E}\varepsilon_i^y(t)\varepsilon_i^{yT}(t)$. $\mathbf{C}_i(t)$ is considered to be a 3 x 3 identity coefficient matrix and $\mathbf{L}_{ij}(t)$ is the higher level interconnection matrix of states between ith network user and jth network user.

A. Problem Formulation

In what follows, we formulate the control problem for each user as the minimization of the following stochastic quadratic cost function subject to the network interaction state equation (9) and coordination states in equation (10):

$$J_i = E\left[\lim_{t\to\infty}\frac{1}{t}\sum_{\tau=0}^{t-1}\tilde{\mathbf{x}}_i^T(\tau)\mathbf{Q}_i(\tau)\tilde{\mathbf{x}}_i(\tau) + \mathbf{u}_i^T(\tau)\mathbf{R}_i(\tau)\mathbf{u}_i\right],$$
$$= \lim_{t\to\infty}\frac{1}{t}\sum_{\tau=0}^{t-1}\sum_{\substack{\tilde{\mathbf{x}}_i\in\{\tilde{\mathbf{x}}\} \\ \mathbf{u}_i\in\{\mathbf{u}\}}}\left[\tilde{\mathbf{x}}_i^T(\tau)\mathbf{Q}_i(\tau)\tilde{\mathbf{x}}_i(\tau) + \mathbf{u}_i^T(\tau)\mathbf{R}_i(\tau)\mathbf{u}_i(\tau)\right]\rho_i(\tilde{\mathbf{x}}_i, \mathbf{u}_i)$$

Subject to: equations (9) and (10). (11)

Here, $\mathbf{Q}_i(t) \in \Re^{3\times 3} \geq \mathbf{0}$ is assumed symmetric, positive semi-definite matrix and $\mathbf{R}_i(t) \in \Re^{M\times M} > \mathbf{0}$ is assumed symmetric, positive definite matrix. These matrices are assumed known to the designer and they signify state and control input variables penalty, respectively [18]. In the sequel we choose $\mathbf{Q}_i$ to be an identity matrix and $\mathbf{R}_i$ to be a matrix of unity entries for simplicity. The motivation behind the stochastic quadratic cost function is that it has a robust and fast tracking rate [8] as it trades-off between the size of states and the control action simultaneously. The objective function takes into account both the user and network consideration discussed in (7). The joint probability density function (pdf) $\rho_i(\tilde{\mathbf{x}}_i, \mathbf{u}_i)$ denotes the cross-layer occupation measure (COM). The COM is defined as $\rho_i(\tilde{\mathbf{x}}_i, \mathbf{u}_i) = \Pr(\mathbf{u}_i \mid \tilde{\mathbf{x}}_i) \sum_{\mathbf{u}_i \in \{\mathbf{u}_i\}} \rho_i(\tilde{\mathbf{x}}_i, \mathbf{u}_i)$. It gives the steady state probability that the control system is in state $\tilde{\mathbf{x}}_i \in \{\tilde{\mathbf{x}}\}$ and the driving control parameter $\mathbf{u}_i \in \{\mathbf{u}_i\}$ is chosen [5]. Vector $\tilde{\mathbf{x}}_i$ is of dimension three and is assumed Gaussian distributed [16]. The evaluation of the pdf follows the Gaussian multiple model adaptive estimator (MMAE) of parameters and states proposed by Ormsby *et al.* [16]. Thus, we seek an optimal $\mathbf{u}_i \in \{\mathbf{u}_i\}$ that solves the problem in (11).

B. Optimal Dynamic Power Controller

In order to solve the minimization problem in (11), we introduce Lagrange multipliers $\boldsymbol{\pi}_t^i$ and a state unification (SU) vector $\boldsymbol{\varphi}_{t+1}^i$ to augment the LCS equality in (10) and the MMSS constraint (9) respectively, to the cost function. We then define the dynamic programming value function as

$$V(\tilde{\mathbf{x}}_t^i) = \min_{\{\mathbf{u}_t^i\}} \left\{ \tilde{\mathbf{x}}_t^{iT} \mathbf{Q}_t^i \tilde{\mathbf{x}}_t^i + \mathbf{u}_t^{iT} \mathbf{R}_t^i \mathbf{u}_t^i \right\} + \min_{\{\mathbf{u}_t^i\}} \rho E\left[V\left(-\boldsymbol{\pi}_t^T \mathbf{y}_t^i + \boldsymbol{\pi}_t^T \sum_{\substack{j=1 \\ j\neq i}} \mathbf{L}_t^{ij} \tilde{\mathbf{x}}_t^j + \boldsymbol{\pi}_t^T \boldsymbol{\varepsilon}_t^y \right) \right] + \min_{\{\mathbf{u}_t^i\}} \rho E\left[V\left(\boldsymbol{\varphi}_{t+1}^T \mathbf{A}_t^i \tilde{\mathbf{x}}_t^i + \boldsymbol{\varphi}_{t+1}^T \mathbf{B}_t^i \mathbf{u}_t^i + \boldsymbol{\varphi}_{t+1}^T \mathbf{C}_t^i \mathbf{y}_t^i + \boldsymbol{\varphi}_{t+1}^T \boldsymbol{\varepsilon}_t^x \right) \right]. \quad (12)$$

Let us postulate a quadratic form for the value function, in which $\mathbf{P}$ is an idempotent matrix so $\mathbf{P}^T = \mathbf{P}$,

$$V(\tilde{\mathbf{x}}_t^i) = \tilde{\mathbf{x}}_t^{iT} \mathbf{P} \tilde{\mathbf{x}}_t^i + \mathbf{D} \quad . \quad (13)$$

We can proceed by substituting this form (with as yet undetermined matrices $\mathbf{P}$ and $\mathbf{D}$) into the value function (12). For convenience of notation, we drop the time slot subscripts and the subsystem superscripts. In all cases, $\tilde{\mathbf{x}}$, $\mathbf{u}$, $\mathbf{y}$, $\boldsymbol{\pi}$, $\boldsymbol{\varphi}$ and $\boldsymbol{\varepsilon}$ refer to time slot t dated variables corresponding to the ith subsystem.

$$V(\tilde{\mathbf{x}}) = \min_{\mathbf{u}} \left\{ \tilde{\mathbf{x}}^T \mathbf{Q} \tilde{\mathbf{x}} + \mathbf{u}^T \mathbf{R} \mathbf{u} \right\} + \rho \mathbf{D} + \min_{\mathbf{u}} \rho E\left[V\left(-\boldsymbol{\pi}^T \mathbf{y} + \boldsymbol{\pi}^T \sum_{\substack{j=1 \\ j\neq i}} \mathbf{L}^{ij} \tilde{\mathbf{x}}^j + \boldsymbol{\pi}^T \boldsymbol{\varepsilon}^y \right) \right] + \min_{\mathbf{u}} \rho E\left[\left(\boldsymbol{\varphi}^T \mathbf{A}\tilde{\mathbf{x}} + \boldsymbol{\varphi}^T \mathbf{B}\mathbf{u} + \boldsymbol{\varphi}^T \mathbf{C}\mathbf{y} + \boldsymbol{\varphi}^T \boldsymbol{\varepsilon}^x \right)^T \mathbf{P} \left(\boldsymbol{\varphi}^T \mathbf{A}\tilde{\mathbf{x}} + \boldsymbol{\varphi}^T \mathbf{B}\mathbf{u} + \boldsymbol{\varphi}^T \mathbf{C}\mathbf{y} + \boldsymbol{\varphi}^T \boldsymbol{\varepsilon}^x \right) \right] \quad (14)$$

Expanding the quadratic terms in the brackets and noting that $\left(\boldsymbol{\varphi}^T \mathbf{A}\, \mathbf{x}\right)^T = \mathbf{x}^T \mathbf{A}^T \boldsymbol{\varphi}$. Also, the expected value of the stochastic shocks is zero so terms of the form: $\tilde{\mathbf{x}}^T \mathbf{A}^T \boldsymbol{\varphi} \mathbf{P} \boldsymbol{\varphi}^T \boldsymbol{\varepsilon}^x$, $\mathbf{u}^T \mathbf{B}^T \boldsymbol{\varphi} \mathbf{P} \boldsymbol{\varphi}^T \boldsymbol{\varepsilon}^x$, $\mathbf{y}^T \mathbf{C}^T \boldsymbol{\varphi} \mathbf{P} \boldsymbol{\varphi}^T \boldsymbol{\varepsilon}^x$, $\boldsymbol{\varepsilon}^{xT} \boldsymbol{\varphi} \mathbf{P} \boldsymbol{\varphi}^T \mathbf{A}\tilde{\mathbf{x}}$, $\boldsymbol{\varepsilon}^{xT} \boldsymbol{\varphi} \mathbf{P} \boldsymbol{\varphi}^T \mathbf{B}\mathbf{u}$, and $\boldsymbol{\varepsilon}^{xT} \boldsymbol{\varphi} \mathbf{P} \boldsymbol{\varphi}^T \mathbf{C}\mathbf{y}$ drop out. We are left with

$$V(\tilde{\mathbf{x}}) = \min_{\mathbf{u}} \left\{ \tilde{\mathbf{x}}^T \mathbf{Q} \tilde{\mathbf{x}} + \mathbf{u}^T \mathbf{R} \mathbf{u} \right\} + \rho \mathbf{D} + \min_{\mathbf{u}} \rho E\left[V\left(-\boldsymbol{\pi}^T \mathbf{y} + \boldsymbol{\pi}^T \sum_{\substack{j=1 \\ j\neq i}} \mathbf{L}^{ij} \tilde{\mathbf{x}}^j + \boldsymbol{\pi}^T \boldsymbol{\varepsilon}^y \right) \right] + \min_{\mathbf{u}} \rho E \begin{bmatrix} \tilde{\mathbf{x}}^T \mathbf{A}^T \boldsymbol{\varphi} \mathbf{P} \boldsymbol{\varphi}^T \mathbf{A}\tilde{\mathbf{x}} + \tilde{\mathbf{x}}^T \mathbf{A}^T \boldsymbol{\varphi} \mathbf{P} \boldsymbol{\varphi}^T \mathbf{B}\mathbf{u} + \tilde{\mathbf{x}}^T \mathbf{A}^T \boldsymbol{\varphi} \mathbf{P} \boldsymbol{\varphi}^T \mathbf{C}\mathbf{y} \\ + \mathbf{u}^T \mathbf{B}^T \boldsymbol{\varphi} \mathbf{P} \boldsymbol{\varphi}^T \mathbf{A}\tilde{\mathbf{x}} + \mathbf{u}^T \mathbf{B}^T \boldsymbol{\varphi} \mathbf{P} \boldsymbol{\varphi}^T \mathbf{B}\mathbf{u} + \mathbf{u}^T \mathbf{B}^T \boldsymbol{\varphi} \mathbf{P} \boldsymbol{\varphi}^T \mathbf{C}\mathbf{y} \\ + \mathbf{y}^T \mathbf{C}^T \boldsymbol{\varphi} \mathbf{P} \boldsymbol{\varphi}^T \mathbf{A}\tilde{\mathbf{x}} + \mathbf{y}^T \mathbf{C}^T \boldsymbol{\varphi} \mathbf{P} \boldsymbol{\varphi}^T \mathbf{B}\mathbf{u} + \mathbf{y}^T \mathbf{C}^T \boldsymbol{\varphi} \mathbf{P} \boldsymbol{\varphi}^T \mathbf{C}\mathbf{y} \\ + \boldsymbol{\varepsilon}^{xT} \boldsymbol{\varphi} \mathbf{P} \boldsymbol{\varphi}^T \boldsymbol{\varepsilon}^x \end{bmatrix}. \quad (15)$$

The optimal control strategy from (15) implies,

$\mathbf{u}^* = -\left(\mathbf{R} + \rho \mathbf{B}^T \boldsymbol{\varphi} \mathbf{P} \boldsymbol{\varphi}^T \mathbf{B}\right)^{-1} \rho \mathbf{B}^T \boldsymbol{\varphi} \mathbf{P} \boldsymbol{\varphi}^T \mathbf{A}\tilde{\mathbf{x}}$. Or, more succinctly,

$\mathbf{u}^* = -\mathbf{F}\tilde{\mathbf{x}}$, with $\mathbf{F} = \left(\mathbf{R} + \rho \mathbf{B}^T \boldsymbol{\varphi} \mathbf{P} \boldsymbol{\varphi}^T \mathbf{B}\right)^{-1} \rho \mathbf{B}^T \boldsymbol{\varphi} \mathbf{P} \boldsymbol{\varphi}^T \mathbf{A}$. (16)

We note from (16) that the optimal control strategy requires the input control vector to react linearly to the interaction state vector $\tilde{\mathbf{x}}$. First order conditions for optimality of other variables are [20]:

$$\frac{\partial V(\tilde{\mathbf{x}})}{\partial \boldsymbol{\pi}} = \rho V_{\boldsymbol{\pi}} \left(\mathbf{y} - \sum_{\substack{j=1 \\ j\neq i}} \mathbf{L}^{ij} \tilde{\mathbf{x}}_j - \boldsymbol{\varepsilon}^y \right) = 0 \text{ ,with } V_{\boldsymbol{\pi}} = \frac{\partial V(\tilde{\mathbf{x}})}{\partial \boldsymbol{\pi}} \quad . \quad (17)$$

$$\frac{\partial V(\tilde{\mathbf{x}})}{\partial \mathbf{y}} = V_{\mathbf{y}}(\boldsymbol{\pi}) + \mathbf{C}^T \boldsymbol{\varphi} \mathbf{P} \boldsymbol{\varphi}^T \mathbf{A}\tilde{\mathbf{x}} + \mathbf{C}^T \boldsymbol{\varphi} \mathbf{P} \boldsymbol{\varphi}^T \mathbf{B}\mathbf{u} + 2\mathbf{C}^T \boldsymbol{\varphi} \mathbf{P} \boldsymbol{\varphi}^T \mathbf{C}\mathbf{y} = 0 \quad (18)$$

$$\frac{\partial V(\tilde{\mathbf{x}})}{\partial \boldsymbol{\varphi}} = \left(\tilde{\mathbf{x}}^T \mathbf{A}^T \mathbf{P} \mathbf{A} + \mathbf{u}^T \mathbf{B}^T \mathbf{P} \mathbf{A} + \mathbf{y}^T \mathbf{C}^T \mathbf{P} \mathbf{A}\right) \tilde{\mathbf{x}} + \left(\tilde{\mathbf{x}}^T \mathbf{A}^T \mathbf{P} \mathbf{B} + \mathbf{u}^T \mathbf{B}^T \mathbf{P} \mathbf{B} + \mathbf{y}^T \mathbf{C}^T \mathbf{P} \mathbf{B}\right) \mathbf{u} + \left(\tilde{\mathbf{x}}^T \mathbf{A}^T \mathbf{P} \mathbf{C} + \mathbf{u}^T \mathbf{B}^T \mathbf{P} \mathbf{C} + \mathbf{y}^T \mathbf{C}^T \mathbf{P} \mathbf{C}\right) \mathbf{y} + \boldsymbol{\varepsilon}^{xT} \mathbf{P} \boldsymbol{\varepsilon}^x = 0 = \tilde{\mathbf{x}}_{t+1}, \quad \tilde{\mathbf{x}}(0) = \tilde{\mathbf{x}}_0 . \quad (19)$$

$$\frac{\partial V(\tilde{\mathbf{x}})}{\partial \tilde{\mathbf{x}}} = \left(\mathbf{Q} + \rho \mathbf{A}^T \boldsymbol{\varphi} \mathbf{P} \boldsymbol{\varphi}^T \mathbf{A}\right) \tilde{\mathbf{x}} + \left(\rho \mathbf{A}^T \boldsymbol{\varphi} \mathbf{P} \boldsymbol{\varphi}^T \mathbf{B}\right) \mathbf{u} + \left(\rho \mathbf{A}^T \boldsymbol{\varphi} \mathbf{P} \boldsymbol{\varphi}^T \mathbf{C}\right) \mathbf{y} = 0 = \boldsymbol{\varphi}_t \ , \boldsymbol{\varphi}(\infty) = \boldsymbol{\varphi}_\infty \ . \quad (20)$$

Equations (19) and (20) are a two-point boundary value problem (TPBVP). The TPBVP must be satisfied by an input control sequence $\{\mathbf{u}\}$ in (16) in order to have a stationary value of the value function (12). We demonstrate that the linear policy function in (16) (derived from a postulated quadratic value function) does actually imply a quadratic value function. In the process, we will be able to determine the two matrices $\mathbf{P}$ and $\mathbf{D}$. To do this, we substitute the policy function $\mathbf{u}^* = -\mathbf{F}\tilde{\mathbf{x}}$ back into the value function (12). Note that $-\tilde{\mathbf{x}}^T\mathbf{F}^T\mathbf{B}^T\mathbf{P}\mathbf{A}\tilde{\mathbf{x}}$ is a scalar and so equal to $-\tilde{\mathbf{x}}^T\mathbf{A}^T\mathbf{P}\mathbf{B}\mathbf{F}\tilde{\mathbf{x}}$. Also, the postulated quadratic value function in (13) is assumed independent of any state variable [12]. Thus, from (15) we have

$$V(\tilde{\mathbf{x}}) = \tilde{\mathbf{x}}^T\mathbf{P}\tilde{\mathbf{x}} + \mathbf{D} = \begin{bmatrix} \tilde{\mathbf{x}}^T\mathbf{Q}\tilde{\mathbf{x}} + \tilde{\mathbf{x}}^T\mathbf{F}^T\mathbf{Q}\mathbf{F}\tilde{\mathbf{x}} \\ +\rho E\begin{pmatrix} \tilde{\mathbf{x}}^T\mathbf{A}^T\mathbf{P}\mathbf{A}\tilde{\mathbf{x}} - 2\tilde{\mathbf{x}}^T\mathbf{A}^T\mathbf{P}\mathbf{B}\mathbf{F}\tilde{\mathbf{x}} \\ +\tilde{\mathbf{x}}^T\mathbf{F}^T\mathbf{B}^T\mathbf{P}\mathbf{B}\mathbf{F}\tilde{\mathbf{x}} \end{pmatrix} + \\ \rho E\boldsymbol{\varepsilon}^{xT}\mathbf{P}\boldsymbol{\varepsilon}^x + \rho\mathbf{D} \end{bmatrix}. \tag{21}$$

Comparing coefficients on constant terms in (21),
$\mathbf{D} = \rho E\boldsymbol{\varepsilon}^{xT}\mathbf{P}\boldsymbol{\varepsilon}^x + \rho\mathbf{D}$. Simplifying this equation by applying the result $E\boldsymbol{\varepsilon}^{xT}\mathbf{P}\boldsymbol{\varepsilon}^x = tr\left(E\boldsymbol{\varepsilon}^{xT}\mathbf{P}\boldsymbol{\varepsilon}^x\right) = tr\left(\mathbf{P}E\boldsymbol{\varepsilon}^{xT}\boldsymbol{\varepsilon}\right) = tr\left(\mathbf{P}\Theta_{\varepsilon}\right)$, we have

$$\mathbf{D} = \frac{\rho}{1-\rho}tr\left(\mathbf{P}\Theta_{\varepsilon}\right). \tag{22}$$

This equation shows how the additive uncertainty caused by the stochastic shocks $\boldsymbol{\varepsilon}_t$, does have an effect on the value function, but this effect is limited to the constant term, which is independent of the policy.
Comparing coefficients on the terms quadratic in $\tilde{\mathbf{x}}$ from (21), we have

$$\mathbf{P} = \mathbf{Q} + \mathbf{F}^T\mathbf{R}\mathbf{F} + \rho\left(\mathbf{A}^T\mathbf{P}\mathbf{A} - 2\mathbf{A}^T\mathbf{P}\mathbf{B}\mathbf{F} + \mathbf{F}^T\mathbf{B}^T\mathbf{P}\mathbf{B}\mathbf{F}\right). \tag{23}$$

Rearranging,

$$\mathbf{P} = \mathbf{Q} + \rho\mathbf{A}^T\mathbf{P}\mathbf{A} - 2\rho\mathbf{A}^T\mathbf{P}\mathbf{B}\mathbf{F} + \mathbf{F}^T\left(\mathbf{R} + \rho\mathbf{B}^T\mathbf{P}\mathbf{B}\right)\mathbf{F},$$

$$= \mathbf{Q} + \rho\mathbf{A}^T\mathbf{P}\mathbf{A} - \rho^2\mathbf{A}^T\mathbf{P}\mathbf{B}\left(\mathbf{R} + \rho\mathbf{B}^T\mathbf{P}\mathbf{B}\right)^{-1}\mathbf{B}^T\mathbf{P}\mathbf{A}. \tag{24}$$

Here, $\mathbf{F} = \left(\mathbf{R} + \rho\mathbf{B}^T\mathbf{P}\mathbf{B}\right)^{-1}\rho\mathbf{B}^T\mathbf{P}\mathbf{A}$, is independent on state unification weighting vector $\boldsymbol{\varphi}$.

Equation (24) confirms that a linear policy function does imply a quadratic value function. It is often known as the discrete in time algebraic matrix Riccati equation (DARE). This matrix is a non linear problem so we simply use an iterative technique based on a matrix Riccati difference equation to solve the $\mathbf{P}$ matrix. Starting from an initial guess of $\mathbf{P}$ matrix in the value function, $\mathbf{P}_k$ is updated to $\mathbf{P}_{k+1}$ according to

$$\mathbf{P}_{k+1} = \mathbf{Q} + \rho\mathbf{A}^T\mathbf{P}_k\mathbf{A} - \rho^2\mathbf{A}^T\mathbf{P}_k\mathbf{B}\left(\mathbf{R} + \rho\mathbf{B}^T\mathbf{P}_k\mathbf{B}\right)^{-1}\mathbf{B}^T\mathbf{P}_k\mathbf{A}. \tag{25}$$

This equation is iterated until convergence, which is guaranteed to uniqueness under very mild weak conditions. That is, having eigenvalues in $\mathbf{A}$ of modulus less than unity is a sufficient condition [12].

At this stage it is worthy of note that discrete equations (19) and (20) contain the lower level variables namely, $\mathbf{u}$ and $\tilde{\mathbf{x}}$ as well as higher level unification variables (UV) namely, $\mathbf{y}$, $\boldsymbol{\varphi}$, and $\boldsymbol{\pi}$. Hitherto, $\mathbf{y}$ signifies states from other UCGs, $\boldsymbol{\varphi}$ and $\boldsymbol{\pi}$ signify the *unification weight vectors* such as energy reserves and information from higher layers and $\tilde{\mathbf{x}}$ signifies the *interaction vector* of states between UCGs. Consequently, we outline PMMUP operation [34] and suggest MRSUP Algorithm. MRSUP stands for synchronous (and asynchronous) multi-radio multi-channel states unification variables prediction (MRSUPS and MRSUPA). MRSUPA and MRSUPS solve the power optimization with $\mathbf{y}$ and $\boldsymbol{\varphi}$ as the unification variables.

C. PMMUP Operation

Power Selection Process: The PMMUP at the Link Layer chooses initial probing power and broadcasts messages to all interfaces. This fraction of maximum power level is vital for neighbour discovery process with low network flooding effects. The PMMUP then performs power selection coordination as summarized in Algorithm 1. We refer to the total probing power over the interfaces as *tot-ProbPow*. The energy residing in a node is referred to as *Energy Reserves*.

Algorithm 1: Summary of Energy-Efficient Power Selection

1. If (*tot-ProbPow > the Energy Reserves* and *Load Queue = 0 at the NICs)*
2. Each NIC selects transmission power to zero.
3: else
4: PMMUP unicasts and/or multicasts "ps-Request" message
5: Neighbour NICs evaluate "Link State Information" and feedback "ps-Ack"
6: Sender NICs receive "ps-Ack" and evaluate "Link State Information"
7: Each sender NIC runs local power optimization algorithm (Cf. Section IVD)
8: Each NIC unicasts pending DATA traffic to the Neighbour Destinations
9: Each sender NIC copies the optimal power values to the PMMUP table
10: endif

PMMUP requests its neighbours for link state information by unicasting power selection (i.e., ps-Request) message. Up on receiving "ps-Request" messages, neighbouring NICs evaluate the "link state information" such as SINR, Interference, Rate, Queue status and Energy reserves (i.e., line 5). After receiving the acknowledgement (i.e., ps-Ack) message, each sender NIC evaluates additional state information such as Round trip time (RTT) (i.e., line 6). Transmission power is then optimally selected based on the link state information (i.e., line 7). Data traffics are transmitted using optimal power levels (i.e., line 8) and the PMMUP table is updated for the next time slot (i.e., line 9).

D. PMMUP based Power Control Algorithm

Algorithm 2: MRSUP: Unification States Based Transmission Power Optimization

Input: $\boldsymbol{\varphi}$, $\mathbf{y}$; $\tilde{\mathbf{x}}_i$; ***A, B, C, Q*** *and* ***R***

Output: $\mathbf{u}_i^*$ */*ith user optimal power control signal*/*

1: **while** $(k \geq 1)$ **do**
2: **for each** *(user* $i \in [1, N]$*)* **do**
3: **Predict:** $\tilde{\mathbf{x}}_i(k) \leftarrow \tilde{\mathbf{x}}_i(k+1)$; $\boldsymbol{\varphi}_i(k) \leftarrow \boldsymbol{\varphi}_i(k+1)$;
4: **if** $(\tilde{\mathbf{x}}_i(k+1) \equiv \tilde{\mathbf{x}}_i^*$ && $\boldsymbol{\varphi}_i(k) \leftarrow \boldsymbol{\varphi}_i(k+1)$ **for any** $i \neq j$, $\forall j \in [1, N]$);
5: **else if** $(\tilde{\mathbf{x}}_i(k+1) \equiv \tilde{\mathbf{x}}_i^*$ && $\boldsymbol{\varphi}_i(k) \leftarrow \boldsymbol{\varphi}_i(k+1)$ **for all** $\forall i \in [1, N]$) ;
6: **Update PMMUP table**: $\mathbf{y}(k) \leftarrow \mathbf{y}(k+1)$*;*
7: **if** *(* $e(k+1) \leq \varepsilon_{rr}$ *, a small positive value);*
8: **Compute:** $\mathbf{u}_i^* = f(\boldsymbol{\varphi}_i^*, \tilde{\mathbf{x}}_i^*, \mathbf{y}_i^*) = -\mathbf{F}_{\boldsymbol{\varphi}} \tilde{\mathbf{x}}_i^*$ */*Eq. (16)*/*
9: **Add:** $\mathbf{u}_i^*$ to Equation (3).
10: **else**
11: **Repeat:** Steps 2-6.
12: **end if**
13: **end for each**
14: **end while**

Here,

$$e(k+1) = \left\| \mathbf{g}(k+1) - \mathbf{g}(k) \right\| \text{, with}$$

$$\mathbf{g}(t) = \left[\mathbf{y}_i^T(k)\ \boldsymbol{\varphi}_i^T(k) \right]^T$$

and

$$\mathbf{g}(k+1) = \left[\mathbf{y}_i^T(k+1)\ \boldsymbol{\varphi}_i^T(k+1) \right]^T .$$

Each user predicts the local link state information as well as the higher layers multi-radio unification variables such as energy reserves for packet transmission (i.e., line 1-3). If the prediction convergence rate is not the same for all users then MRSUP algorithm converges *asynchronously*, otherwise *synchronously* (i.e., line 4-5). Using such state trajectories, the coordination variables are updated at the PMMUP table (i.e., line 6). Optimal power control signal is then computed using the converged state trajectories (i.e., line 8).

After computing the optimal power control signal $u_i^*(t) = U\,\mathbf{u}_i^*(t)$, where $U = [1]$ (i.e., for each user), the optimal dynamic power control law becomes

$$p_i(t+1) = p_i(t) + f_i(\mathbf{x}) + u_i^*(t) . \tag{26}$$

The optimal law is constrained by $0 \leq \sum_{i \in \{1,\ldots,N\}} p_i(t+1) \leq p_{MP}^{sum}$, where $p_{MP}^{sum} \leq p_{MP}^{\max}$ are sum and maximum powers at each mesh point (MP) node.

Clearly, the local solutions for $\tilde{\mathbf{x}}$ depend on the converged *DARE* $\mathbf{P}$ matrix. Variables $\tilde{\mathbf{x}}$ and $\boldsymbol{\varphi}$ are functions of the coordination variable $\mathbf{y}$ from the PMMUP. Asynchronous convergence of the MRSUP may become non-trivial.

E. Convergence Analysis

Theorem 1: Suppose the *k*th asynchronous iteration of the interaction and unification state equations for the *i*th user can be written in the form

$$\tilde{\mathbf{x}}_i^{(k+1)} = \left(\tilde{\mathbf{x}}_i^T\ \mathbf{u}_i^T\ \mathbf{y}_i^T \right)^{(k)} \begin{pmatrix} \mathbf{A}^T\mathbf{PA} & \mathbf{A}^T\mathbf{PA} & \mathbf{A}^T\mathbf{PC} \\ \mathbf{B}^T\mathbf{PA} & \mathbf{B}^T\mathbf{PB} & \mathbf{B}^T\mathbf{PC} \\ \mathbf{C}^T\mathbf{PA} & \mathbf{C}^T\mathbf{PB} & \mathbf{C}^T\mathbf{PC} \end{pmatrix} \begin{pmatrix} \tilde{\mathbf{x}}_i^{(k)} \\ \mathbf{u}_i^{(k)} \\ \mathbf{y}_i^{(k)} \end{pmatrix} + \boldsymbol{\varepsilon}_i^{xT(k)} \mathbf{P} \boldsymbol{\varepsilon}_i^{x(k)}$$

with $\tilde{\mathbf{x}}_i^{(0)} = 0$, $\mathbf{y}_i^{(k)} = \sum_{\substack{j=1 \\ j \neq i}}^{N} \mathbf{L}_{ij}^{(k)} \mathbf{w}_{\mathbf{x}j}^{(k)} + \boldsymbol{\varepsilon}_j^{(k)}$. (27)

Or, more succinctly,

$$\tilde{\mathbf{x}}_i^{(k+1)} = \mathbf{z}_{\mathbf{x}i}^{T(k)}\ \mathbf{P}_{\mathbf{x}}\ \mathbf{z}_{\mathbf{x}i}^{(k)} + \boldsymbol{\varepsilon}_i^{xT} \mathbf{P} \boldsymbol{\varepsilon}_i^{x\,(k)} . \tag{28}$$

$$\boldsymbol{\varphi}_i^{(k)} = \begin{pmatrix} \mathbf{Q} + \rho \mathbf{A}^T \boldsymbol{\varphi}_i^{(k+1)} \mathbf{P} \boldsymbol{\varphi}_i^{T(k+1)} \mathbf{A} \\ \rho \mathbf{A}^T \boldsymbol{\varphi}_i^{(k+1)} \mathbf{P} \boldsymbol{\varphi}_i^{T(k+1)} \mathbf{B} \\ \rho \mathbf{A}^T \boldsymbol{\varphi}_i^{(k+1)} \mathbf{P} \boldsymbol{\varphi}_i^{T(k+1)} \mathbf{C} \end{pmatrix} \begin{pmatrix} \tilde{\mathbf{x}}_i^{(k)} \\ \mathbf{u}_i^{(k)} \\ \mathbf{y}_i^{(k)} \end{pmatrix} \text{, with } \boldsymbol{\varphi}_i^{(K)} = 0 ,$$

$$\mathbf{y}_i^{(k)} = \sum_{\substack{j=1 \\ j \neq i}}^{N} \mathbf{L}_{ij}^{(k)} \mathbf{w}_{\boldsymbol{\varphi}j}^{(k)} + \boldsymbol{\varepsilon}_j^{(k)} . \tag{29}$$

Or, more succinctly,

$$\boldsymbol{\varphi}_i^{(k)} = \mathbf{P}_{\boldsymbol{\varphi}}^{(k+1)} \mathbf{z}_{\boldsymbol{\varphi}i}^{(k)} . \tag{30}$$

(a) The MRSUPA algorithm satisfies a contraction property defined on a space S whereby

$$S = \sum_{i=1}^{N} S_i , \quad S_i = C_d\left([k_0, k_\infty]; \square^{2ni} \right), \tag{31}$$

and $C_d(.)$ denotes the set of discrete functions.

(b) MRSUPA algorithm converges.

(c) The rate of convergence depends on iteration interval and the interaction between users on separate UCGs.

Proof 1: Appendix A.

V. Simulation Environment And Results

In our simulations, we used MATLAB™ version 7.1[35]. We assumed 50 stationary wireless nodes randomly located in a 1200 m x 1200 m region. Each node had 4 NICs each tuned to a unique UCG. Each UCG had 50 NICs assumed fully interconnected over a wireless medium. For evaluation purposes, we considered the frequency spectrum of 2412 MHz-2472 MHz. So that each UCG consisted of frequency carriers: 2427 MHz, 2442 MHz, 2457 MHz and 2472 MHz. Other simulation specifications were used as illustrated in Table III.

TABLE III
SIMULATION SPECIFICATIONS

Parameter	*Specs.*	*Parameter*	*Specification*
Bandwidth	10 *MHz*	Transmission &	240 m and 480 m

		Interfererence Ranges	
Basic Rate	2 *Mbps*	Probing power	Variable [Pmin,Pmax]
Maximum Link Capacity	54 *Mbps*	MAC Scheme	Time-Slotted CDMA
Minimum Transmit Power	10 *mW*	Slot duration and Power update	100 msec, 80 msec
SINR threshold	4-10 *dB*	Offered Load and Queue Length	12.8,51.2,89.6,128 *packets/s and* 50 *packets*
Thermal Noise	90 *dBm*	Packet sizes and FEC sizes	1000 *bytes and 50 bytes*
Maximum Transmit Power	500 *mW*	Simulation Time	60 *seconds*

In order to evaluate the system matrix **A,** the channel gain and the interference are estimated as follows: At each user belonging to UCG l, the channel gain conditions are given by [19]

$$G_{ll} = L(d_0)\left(\frac{d_{ll}}{d_0}\right)^{-\upsilon} Y_l\left(X_{Il}^2 + X_{Ql}^2\right), \qquad (32)$$

where $L(d_0) = \frac{\hbar_i \hbar_r \varpi^2}{16\pi^2 d_0^2}$ is the path loss of the close-in distance d_0, $\hbar_i, \hbar_r$ are the antenna gains of the transmitter NIC and the receiver NIC assumed unity, respectively, and ϖ is the wavelength of the carrier signal. Let the close-in distance be $d_0 = 100$ meters and d_{ll} be the distance between the transmitter i and neighbourhood receiver r on UCG l. The parameters $Y_l \quad \forall l$ are i.i.d. lognormal shadowing distributed random variables with the standard deviation σ_s, set to 8 dB. The random variables X_{Il} and X_{Ql} are the zero mean and variance 0.5 real and imaginary components, respectively of a Rayleigh fading channel gains. The path loss exponent (PLE) υ is assumed to be $2 \le \upsilon \le 6$, depending on the physical environment conditions. Using the channel autocorrelation function in [7] and assuming mobility-limited mesh devices then $\sigma_m^2 = \sigma_s^2\left(1 - a^2\right)$, whereby picking $a = 0.95$ yields $\sigma_m = 1.56$ dB for equation (6). Using equation (1) and [6] we approximate interference as

$$\tilde{I}_{(i,r),l}(t+1) \approx \tilde{I}_{(i,r),l}(t) + n(t), \qquad (33)$$

where $\tilde{I}_{(i,r),l}(t)$ is the bidirectional form of equation (1). The term $n(t)$ is a unit mean noise with variance σ_m^2 = 1.56 dB. Suppose the network is considered to operate close to steady state then interference becomes time-invariant. The time-invariant effective channel gain becomes,

$$\lim_{t\to\infty} \frac{1}{t}\sum_{\tau=0}^{t-1} \mathrm{E}\left[\frac{G_{ll}}{\tilde{I}_{(i,r),l}}\right](\tau) = H \ . \qquad (34)$$

Other model matrices e.g., **B, C, R,** and **Q** were generated as defined in Section IV. We set α_β, α_I, α_Γ to be unity and user and network centric weights ω_{l1} and ω_{l2} both to be 0.5. The steady state probability parameter ρ set to be 0.5.

Figure 3 depicts the per-link (a simple case) experimental setup for power optimization. A Similar setup illustrates communication process between an MRMC node with its neighbours in the entire mesh network. Two sessions depicted by the diagram are concurrent. Performance investigations were based on Monte Carlo simulations. For each random network configuration several independent Monte Carlo runs were carried out.

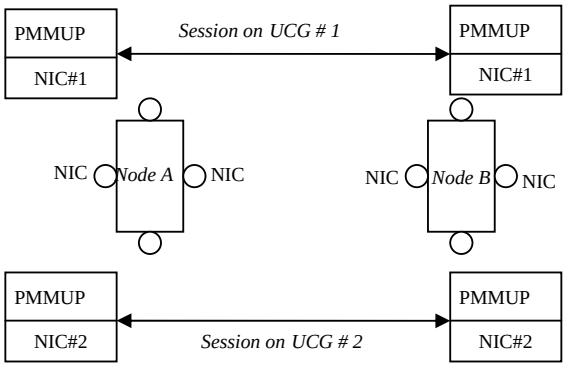

Fig. 3: An experimental set up for a 2 node case: Node A and Node B.

For a single unified channel graph (UCG) and time slot, packets were transmitted by each NIC to a target receiver NIC. The consumed transmission power for duration of time slot was plotted as shown in Fig. 4. The consumed transmission powers were recorded for different channel conditions depicted by the effective channel gain, *H*. It can be observed that as the number of packets transmitted during each time slot increases the amount of transmission energy needed to 'carry' the packets increases linearly (see Fig. 4). Bad (lossy) channel conditions, i.e., *H* = 0.2 requires additional transmission powers compared to ideal (favourable) channel conditions, i.e., *H* = 1. In order to transmit 500 packets in every time slot, transmissions when H = 1 offered about 400%, 150%, 10%, 5% more power saving than when H = 0.2, 0.4, 0.6 and 0.8, respectively. Lossy channels are as a result of wireless channel fading and interferences caused by multiple transmissions over a common medium. To study effects of a practical wireless channel scenario, we assumed an effective channel gain of 0.4 for subsequent simulations.

In Fig. 5, the power selection multi-radio multi-channel unification protocol (PMMUP) based algorithm described in Section IVD was tested for convergence. Simulations were run for a local UCG of carrier frequency 2427 MHz with an adjacent interfering power leakage factor assumed to be 0.5. Simulations were carried out for the duration of a time slot so that convergence rate could be measured within a fraction of the time slot. At an iteration sample of three, MRSUPA yields on average 40% and 50% faster convergence than MRSUPS and Effective band interference estimation based dynamic power control (EBIA) [4], [10]. These results are explained as follows: Asynchronous algorithm (e.g., MRSUPA) requires that any NIC or network user which has successfully

completed execution of the channel states and power levels proceeds to send the pending packets in its queue independent of other NICs and or users. On the other hand synchronous algorithm (e.g., MRSUPS) requires all NICs of a node to complete executions at the same time instant before sending DATA packets. Thus, depending on the respective queue load, state executions of some NICs will converge faster than those of others. This leads to faster convergence rate with MRSUPA than with MRSUPS. Finally, it is be noted that EBIA in [4], [10] autonomously predicts interference influences both at the sender node and the receiver node. Interference signals are assumed to be predicted and estimated using Kalman filter [7]. Bi-directional interference estimations consume significant amount of convergence time. Thus, the convergence time is slightly longer than those of the PMMUP enabled methods.

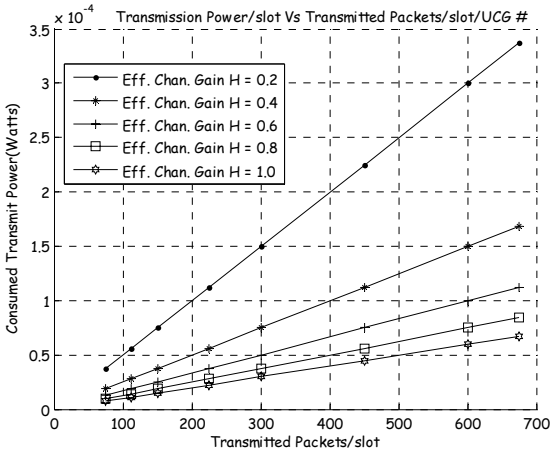

Fig. 4: Rate versus amount of transmitted power per one hop range

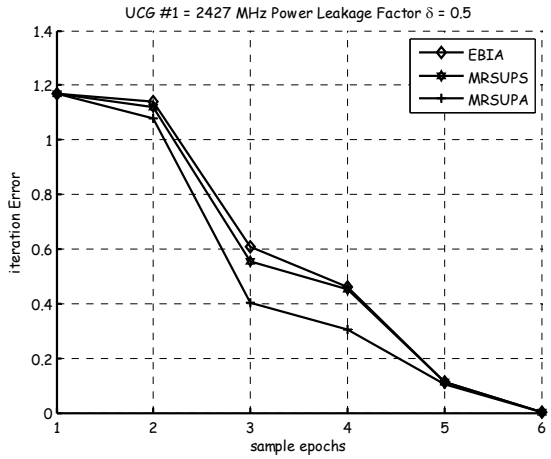

Fig. 5: System convergence speed to steady state

Simulation results revealing how the input control sequence designed in Section IVB drives the unification variables to steady states are shown in Figs. 6 and 7. Results show a multi-radio multi-channel (MRMC) system state response plotted for four UCGs. It was noted that as input control signal drives the MRMC the actual SINR, aggregate interference and transmission rate approaches their respective steady state values. It was observed that despite the unstable initial transient region, the system states are stable in the steady states region. For these experiments we simulated MRSUPA and MRSUPS algorithms to demonstrate the multi-radio system state response times. Under the influence of the input control sequences and external noises (random shocks), the MRSUPA algorithm demonstrated a robust response compared to the MRSUPS algorithms. This observation is due to the reason that MRSUPA stops execution asynchronously, while MRSUPS convergence depends on the longest iteration interval of the PMMUP. PMMUP information exchange (influence) causes transient disturbances and consequently longer steady state times.

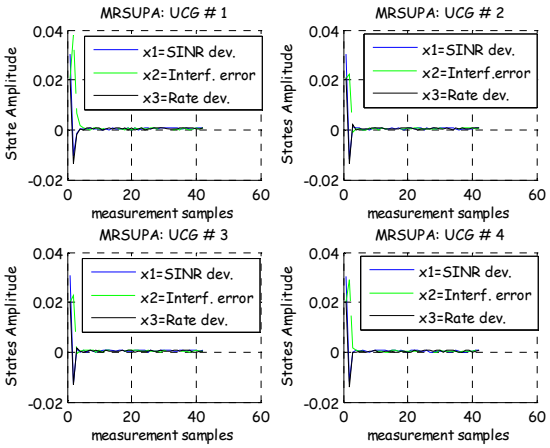

Fig. 6: System State Transition

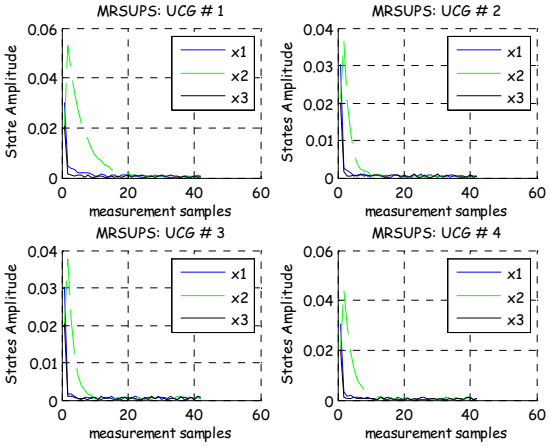

Fig. 7: System State Transition

Figures 8 and 9 depict dynamic power control laws after adding the optimal driving input control sequence to the equation in (3). The simulation tests were carried for an MRMC with four NICs each associated to a unique UCG. Simulation results showed that MRSUPS and MRSUPA algorithms yield monotonically converging transmission power levels as time increases. The converged stationary points represented the optimal power levels during each time slot. Different stationary points were noticed for different independent simulation runs. Independent simulation runs implies different network topologies. Hence inter-node

connectivity optimal power varies in each simulation run. At 15 samples of iteration and on the same channel, the MRSUPA presented 32.54% more power saving than the MRSUPS. The reason being, with MRSUPA network users autonomously terminate state predictions upon convergence and sends the data using a converged transmission power level. On the other hand MRSUPS require that power executions continue as long as other network users have not finished transmission power executions. MRSUPS naturally becomes slightly energy-inefficient than MRSUPA.

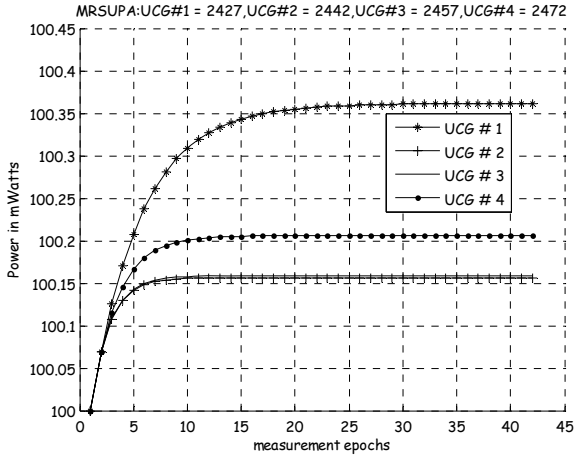

Fig. 8: MRSUPA optimal Power level Selection

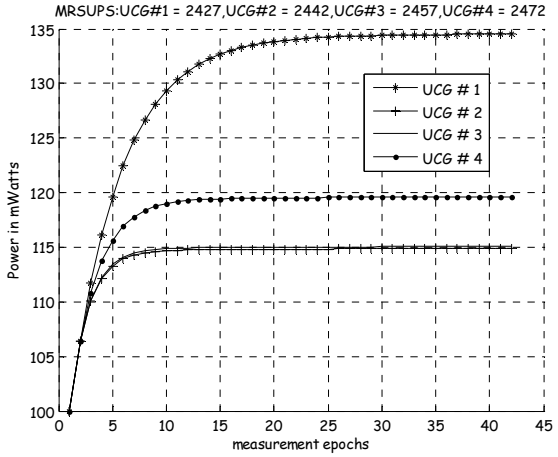

Fig. 9: MRSUPS Optimal Power level Selection

Consider steady state transmission powers responses in Figs. 8 and 9 with the inter-channel power leakage factor of 0.5.

In 60 second simulation time, five Monte Carlo simulation independent runs were performed each depicting a random topology generation. The average hop by hop throughput per multi-radio node versus the offered load at the each queue has been depicted by Fig. 11. These statistical averages were plotted at 95% confidence intervals. The MRSUPA algorithm at cross-channel interference factor of 0.5 was compared with the multi-radio unification protocol (MUP) [25], single channel power controlled network protocol (PCNP) [32] and Effective Band Interference Based Algorithm (EBIA) [4]. It has been observed that on average MRSUPA show most superior average throughput performance of 65.22%, 45.65% and 21.74%, respectively over MUP, PCNP and EBIA at queue load of 51.2 packets per second. The reason is motivated as follows. The MRSUPA scheme exploits at least one power controlled channel per each mesh router node to transmit data traffic. It is predictive and asynchronous, thus fast convergence. It caters for most network states affecting transmission power choice and is managed by Link Layer. Thus, it presents a good trade-off between optimality and complexity. On the other hand, MUP is not power controlled protocol, PCNP is a single channel network which suppresses unidirectional interference at the receiver terminals and EBIA is a single channel which minimizes aggregate network interference as well as increasing SIR level at the receiver.

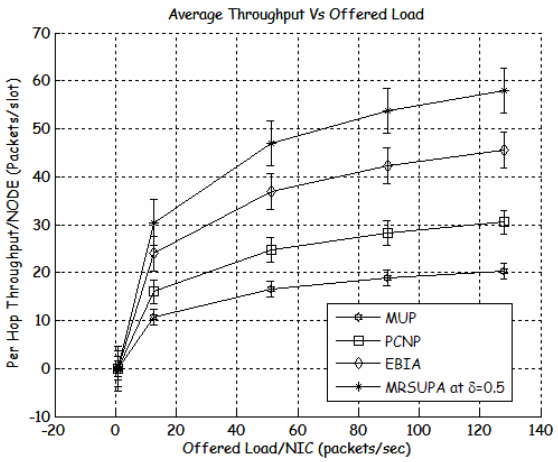

Fig. 11: Per hop Throughput per network Node versus the Offered Load

VI. Conclusion

This work demonstrated the effectiveness of the PMMUP supported dynamic power optimization. Simulation results showed that asynchronous multi-radio multi-channel unification protocol (PMMUP) based algorithms outperform conventional methods in terms of the convergence rate and average throughput performance. However, due to run time overheads, channel assignment and routing were assumed to be static. It would be interesting to efficiently adapt our algorithm to dynamic channel assignment and routing problems in multi-hop multi-radio and multi-channel (MHMRMC) wireless mesh networks. This is the basis of our future work.

APPENDIX A
PROOF OF ASYNCHRONOUS CONVERGENCE

Suppose $\mathbf{W}$ is a matrix of coupling variables between the ith user on UCG l and others [15], [27]. Let $\mathbf{W}$ be a discrete function representing a finite number of users performing a finite number of iterations. We write $\mathbf{W}$ in the form

$$\mathbf{W} = \left[\mathbf{W}_x \quad \mathbf{W}_\varphi \right], \tag{35}$$

where $\mathbf{W}_{\mathbf{x}}$ is the $\tilde{\mathbf{x}}$ component of $\mathbf{W}$ and $\mathbf{W}_{\boldsymbol{\varphi}}$ is the $\boldsymbol{\varphi}$ component of $\mathbf{W}$ given by

$$\mathbf{W}_{\mathbf{x}} = \left[\mathbf{w}_{\mathbf{x}1} \,|\, \mathbf{w}_{\mathbf{x}2} \,|\ldots|\, \mathbf{w}_{\mathbf{x}N}\right], \quad \mathbf{W}_{\boldsymbol{\varphi}} = \left[\mathbf{w}_{\boldsymbol{\varphi}1} \,|\, \mathbf{w}_{\boldsymbol{\varphi}2} \,|\ldots|\, \mathbf{w}_{\boldsymbol{\varphi}N}\right]. \tag{36}$$

Let us consider that each user, $i \in \{1 \ldots N\}$ separately iterates the discrete interaction state equation (28) independent of the unification state equation (30). From (28), we have

$$\tilde{\mathbf{x}}_i^{(k+1)} = \mathbf{z}_{i\mathbf{x}}^{T(k)} \mathbf{P}_{\mathbf{x}} \mathbf{z}_{i\mathbf{x}}^{(k)} + \mathbf{z}_{\mathbf{wx}}^{T(k)} \mathbf{P}_{\mathbf{wx}} \mathbf{z}_{\mathbf{wx}}^{(k)} + \mathbf{P}_{\varepsilon} \boldsymbol{\varepsilon}_i^{x(k)},$$
$$\text{where } \mathbf{z}_{\mathbf{wx}}^{(k)} = \mathbf{y}_{i\mathbf{x}}^{(k)} \text{ and } \mathbf{z}_{i\mathbf{x}}^{(k)} = \left(\tilde{\mathbf{x}}_i^{(k)} \; \mathbf{u}_i^{(k)}\right)^T. \tag{37}$$

At the optimal solution we have

$$\tilde{\mathbf{x}}_i^{*} = \mathbf{z}_{i\mathbf{x}}^{T(*)} \mathbf{P}_{\mathbf{x}} \mathbf{z}_{i\mathbf{x}}^{(*)} + \mathbf{z}_{\mathbf{wx}}^{T(*)} \mathbf{P}_{\mathbf{wx}} \mathbf{z}_{\mathbf{wx}}^{(*)} + \mathbf{P}_{\varepsilon} \boldsymbol{\varepsilon}_i^{x(*)},$$
$$\text{where } \mathbf{z}_{\mathbf{wx}}^{(*)} = \mathbf{y}_{i\mathbf{x}}^{(*)} \text{ and } \mathbf{z}_{i\mathbf{x}}^{(*)} = \left(\tilde{\mathbf{x}}_i^{(*)} \; \mathbf{u}_i^{(*)}\right)^T. \tag{38}$$

Subtracting (38) from (37), applying initial condition $\tilde{\mathbf{x}}_i^{(0)} = 0$, and simplifying we have

$$\mathbf{e}_{i\mathbf{x}}(k) = \mathbf{P}_{\mathbf{wx}} \mathbf{e}_{\mathbf{wx}}(k). \tag{39}$$

Taking the norm of both sides of (39) over the iteration period (k_0, k_∞), we have

$$\max_{k\in[k0,k\infty]} \left\|\mathbf{e}_{i\mathbf{x}}\right\|_2 \le (k_0 - k_\infty) \max_{k\in[k0,k\infty]} \left\|\mathbf{P}_{\mathbf{wx}}\right\|_2 \max_{k\in[k0,k\infty]} \left\|\mathbf{e}_{\mathbf{wx}}\right\|_2. \tag{40}$$

In a similar procedure and noting the final value condition, we define the norm error for the unification state equation as

$$\max_{k\in[k0,k\infty]} \left\|\mathbf{e}_{i\boldsymbol{\varphi}}\right\|_2 \le (k_0 - k_\infty) \max_{k\in[k0,k\infty]} \left\|\mathbf{P}_{\mathbf{w}\boldsymbol{\varphi}}\right\|_2 \max_{k\in[k0,k\infty]} \left\|\mathbf{e}_{\mathbf{w}\boldsymbol{\varphi}}\right\|_2. \tag{41}$$

Combining the inequality (40) and (41) in a compact form for *i*th subsystem, we have

$$\max_{k\in[k0,k\infty]} \begin{pmatrix} \left\|\mathbf{e}_{i\mathbf{x}}\right\|_2 \\ \left\|\mathbf{e}_{i\boldsymbol{\varphi}}\right\|_2 \end{pmatrix} \le (k_0 - k_\infty) \max_{k\in[k0,k\infty]} \begin{pmatrix} \left\|\mathbf{P}_{\mathbf{wx}}\right\|_2 & 0 \\ 0 & \left\|\mathbf{P}_{\mathbf{w}\boldsymbol{\varphi}}\right\|_2 \end{pmatrix} \times \max_{k\in[k0,k\infty]} \begin{pmatrix} \left\|\mathbf{e}_{\mathbf{wx}}\right\|_2 \\ \left\|\mathbf{e}_{\mathbf{w}\boldsymbol{\varphi}}\right\|_2 \end{pmatrix},$$

$$\max_{\substack{k\in[k0,k\infty] \\ i\in[1,N],\ \forall i}} \left\|\mathbf{e}_i(k)\right\|_2 \le (k_0 - k_\infty) \sum_{j=1}^{N} \Phi_{ij} \max_{\substack{k\in[k0,k\infty] \\ j\in[1,N],\ j\ne i}} \left\|\mathbf{e}_{\mathbf{w}j}\right\|_2,$$

$$\max_{\substack{k\in[k0,k\infty] \\ i\in[1,N]}} \left\|\mathbf{e}_i(k)\right\|_2 \le \sigma_i \max_{\substack{k\in[k0,k\infty] \\ j\in[1,N],\ j\ne i}} \left\|\mathbf{e}_{\mathbf{w}j}\right\|_2, \tag{42}$$

$$\sigma_i = (k_0 - k_\infty) \sum_{j\ne i} \Phi_{ij}, \; \mathbf{e}_{\mathbf{w}j} = \left(\mathbf{e}_{\mathbf{wx}j} \;\; \mathbf{e}_{\mathbf{w}\boldsymbol{\varphi}j}\right)^T. \tag{43}$$

(a) If we choose $(k_\infty - k_0)$ such that $\sigma_i < 1$, $\forall i \in [1, N]$, then inequality (42) defines a contraction property on a space S is defined as

$$S = \sum_{i=1}^{N} S_i, \quad S_i = C_d\left([k_0, k_\infty]; \square^{2ni}\right), \tag{44}$$

where $C_d(.)$ denotes the set of discrete functions.

(b) It has been established that satifying a contraction property guarantees the convergence of asynchronous iterations [22].

(c) From (43) the asynchronous convergence depends on the iteration interval $(k_\infty - k_0)$ and the interaction matrix $\Phi_{ij}(k_\infty)$. Each user is not expected to communicate its results after each iteration but only once in an iteration interval. Thus, some users execute more iterations than others. All users of a node share the PMMUP layer and can access state trajectories simultaneously with a reduced effect of communication delay between users on separate UCGs. Hence, such asynchronous algorithm convergences fast.

REFERENCES

[1] I. F. Akyilidiz, X. Wang and W. Wang, "Wireless mesh networks: a survey," Computer Networks, vol. 47, pp. 445-487, 2005.
[2] G. Brar, D. M. Blough, and P. Santi, "Computationally Efficient Scheduling with the Physical interference Model for Throughput Improvement in Wireless Mesh Networks," Proc. MOBICOM'06, Los Angeles, California, USA, 2006. Sept. 23-26.
[3] M. Chiang, "Balancing Transport and Physical Layers in Wireless Multihop Networks: Joint Optimal Congestion and Power Control," IEEE Journal on Selected Areas in Commun., vol. 23, no. 1, pp. 104-116, 2005.
[4] T. O. Olwal, F. O. Aron, B. J. Van Wyk, Y. Hamam, N. Ntlatlapa and M. Odhiambo, "Improved Distributed Dynamic Power Control for Wireless Mesh Networks," In Proc. 7th International Conference, ADHOC-NOW 2008, LNCS 5198, Sophia-Antipolis, France, 2008. Sept. 10-12.
[5] E. Altman, K. Avrachenkov, N. Bonneau, M. Debbah, R. El-Azouzi and D. Menasche, "Constrained Stochastic Games in Wireless Networks," Tech Report, 2007. www-net.cs.umass.edu/~sadoc/mdp
[6] M. Neely, E. Modiano and C. E. Rohrs, "Dynamic Power Allocation and Routing for Time-Varying Wireless Networks," IEEE Journal on Selected Areas in Commun.. vol. 23, no. 1, pp. 89-103, 2005.
[7] K. Shoarinejad, J. L. Speyer, and G. J. Pottie, "Integrated Predictive Power Control and Dynamic Channel Assignment in Mobile Radio Systems," IEEE Trans. on Wireless Commun., vol. 2, no. 5, pp. 976-988, 2003.
[8] A. Subramanian and A. H. Sayed, "Joint Rate and Power Control Algorithms for Wireless Networks," IEEE Trans. On Signal Processing, vol. 53, no. 11, pp. 4204-4214, 2005.
[9] H.-J. Ju and Rubin, "Efficient Backbone Synthesis Algorithm for Multi-Radio Wireless Mesh Networks," Proc. IEEE Wireless Communication and Network Conference, (WCNC) 2006.
[10] S. Sorooshyari and Z. Gajic, "Autonomous Dynamic Power Control for Wireless Networks: User-Centric and Network-Centric Consideration," IEEE Trans. On Wireless Commun., vol. 7, no. 3, pp. 1004-1015, 2008.
[11] K. Wang, C. F. Chiasserini, J. G. Proakis and R. R. Rao, "Joint Scheduling and power control supporting multicasting in wireless ad hoc networks," Ad Hoc Networks, vol. 4, pp. 532-546, 2006.
[12] T. Kailath, A. H. Sayed and B. Hassibi, Linear Estimation, Eaglewood Cliffs, NJ: Prentice Hall, 2000.
[13] M. S. Mahmoud, M. F. Hassan and M. G. Darwish, Large Scale Control Systems Theories and Techniques, Dekkar, New York, 1985.
[14] S. Koskei and Z. Gajic, "Optimal SIR-Based Power Control Strategies for Wireless CDMA Networks," International Journal of Information and Systems Sciences, vol. 1, no. 1, pp. 1-18, 2007.
[15] S. S. Abdelwahed, M. F. Hassan, and M. A. Sultan, "Parallel Asynchronous Algorithms for optimal control of large scale dynamic systems," Journal of Optimal Control Applications and Methods, vol. 18, 1997.
[16] C. D. Ormsby, J. F. Raquet and P. S. Maybeck, "A new generalized residual multiple model adaptive estimator of parameters and states," Mathematical and Computer Modeling, vol. 43, pp. 1092-1113, 2006.
[17] K. Jain, J. Padhye, V. N. Padmanabhan and L. Qiu, "Impact of interference on multi-hop wireless network performance," In Proc. MOBICOM'03, San Diego, California, USA, September 14-19, 2003.

[18] V. Dragan and T. Morozan, "The linear Quadratic Optimization Problem for a class of Discrete-Time Stochastic Linear Systems," International Journal of Innovative Computing, Information and Control, vol. 4, no. 9, pp. 2127-2137, 2008.
[19] T. Shu, M. Krunz and S. Vrudhula, "Joint Optimization of Transmit Power-Time and Bit Energy Efficiency in CDMA Wireless Sensor Networks," Technical Report, TR-UA-ECE-2005-3, April 14, 2005.
[20] R. L. Williams II and D. A. Lawrence, Linear state space controls systems, John Wiley & Sons, Inc., March 2007.
[21] IEEE 802.11s Standard Working Group, Draft amendment available at https://mentor.ieee.org/802.11/public/04/11-04-0662-16-0001-usage-models-tgs.doc.
[22] M. M. El-Tarazi, "Some Convergence results for asynchronous algorithms," Numreish Mathematik, vol. 39, pp. 325-344, 1982.
[23] B. Ata, "Dynamic Power Control in a Wireless Static Channel Subject to a Quality of Service Constraint," Journal of Operation Research, vol. 53, no. 2, pp. 842-841, 2005.
[24] Engim Inc., Multiple Channel 802.11 Chipset. Available from: http://www.engim.com/products_en3000.html.
[25] A. Adya, P. Bahl, J. Padhye, A. Wolman and L. Zhou, "A Multi-Radio Unification Protocol for IEEE 802.11 Wireless Networks," In Proc. first international conference on Broadband Networks (Broadnets'04), 2004.
[26] Mathworks Inc. http://www.mathworks.com/
[27] Z. Gajic and X. Shen, Parallel Algorithms for Optimal Control of Large Scale Linear Systems, Spinger-Verlag, 1993.
[28] J. S. Ishmael, D. Pezaros and N. Race, "Deploying Rural Community Wireless Mesh Networks," IEEE Internet Computing, pp. 22-29, 2008.
[29] S. Merlin, N. Vaidya, and M. Zorzi, "Resource allocation in multi-radio multi-channel multi-hop wireless networks," In Proc. INFOCOM 2008, pp. 610-618.
[30] A. Feistel and S. Stanczak, "Hop by Hop Congestion Control with Power Control for Wireless Mesh Networks," In Proc. IEEE 65th Vehicular Technology Conference (VTC), Dublin, Ireland, April 22-25, pp. 119-123, 2007.
[31] L. Jia, X. Liu, G. Noubir, and R. Rajaman, "Transmission power control for ad hoc wireless networks: throughput, energy and fairness," IEEE Wireless Commun. Network Conference (WCN'05), vol. 1, pp. 619-625, March 2005
[32] P. Li, Q. Shen, Y. Fang and H. Zhang, "Power Controlled Network Protocols for Multi-Rate Ad Hoc Networks," IEEE Trans. Wireless Commun., vol. 8, no. 4, pp. 2142-2149, April 2009.
[33] A. Muqattash and M. Krunz, "Power Controlled dual channel (PCDC) medium access protocol for wireless ad hoc networks," IEEE Intl. Conf. Computer Communications (INFOCOM'03), San Fransisco, CA, USA, March 2003.
[34] T. O. Olwal, F. O. Aron, B. J. Van Wyk, Y. Hamam, P. Siarry, and N. Ntlatlapa, A multiple-State Based Power Control for Multi-Radio Multi-Channel Wireless Mesh Networks," International Journal of Computer Science, vol. 4, no. 1, pp. 53-61, 2009.